Optics Communications 426 (2018) 23–29

Contents lists available at ScienceDirect

Optics Communications

journal homepage: www.elsevier.com/locate/optcom

Method of reducing photon noise and turbulence for laser guide-star detection on large-aperture telescopes

Chao Liu [a,b], Huanyu Xu [a], Lifa Hu [c], Zhaoliang Cao [a,*]

[a] State Key Laboratory of Applied Optics, Changchun Institute of Optics, Fine Mechanics and Physics, Chinese Academy of Sciences, Changchun, 130033, PR China
[b] University of Chinese Academy of Sciences, Beijing, 100039, PR China
[c] School of Science, Jiangnan University, Wuxi, 214122, PR China

ABSTRACT

Adaptive optics systems (AOSs) rely on good estimation of a distorted wavefront. Two problems make centroid detection difficult, namely, the problem of a relatively large subaperture that brings high-order aberrations and that of a large laser guide-star spot that brings in a large photon noise. To solve these problems, we proposed an estimation method based on Poisson statistics to reduce the photon noise, and the high-order aberrations are partly separated from a spot image to well estimate the slope in the subaperture. Simulation results indicate that our method performs better than the weighted center-of-gravity (WCOG) method and correlation method (CM). Under the condition of $SNR = 20$ and $r_0 = 13$cm The root-mean-square values of the residual wavefront using the proposed method are approximately 10%, 50%, and 35% lower than those of the COG, WCOG, and CM, respectively. The proposed method would be highly beneficial for ground-based astronomical AO systems intended to provide moderate to high Strehl ratios at near infrared wavelengths on larger than 10m-aperture telescopes.

1. Introduction

Adaptive optics systems (AOSs) have been widely used in large ground-based telescopes to compensate the aberrations caused by atmospheric turbulence [1,2]. Usually, a Shack–Hartmann wavefront sensor (SHWFS) is utilized in the AOS to detect aberrations. In the AOS of a telescope, the magnitude of the object is mainly limited by the wavefront detection. Therefore, a bright guide star should be selected to detect the aberrations for astronomical AOSs. However, because bright stars in the sky are few, a laser guide star (LGS) is proposed to create a relatively bright star in the sky. However, even if LGS is used to produce a bright artificial star, the photon return remains insufficient for highly precise detection. The photon return would vary according to the telescope site and time of year. As reported from the Gemini South telescope observation, photon return ranges from 10 to 90 ph/(cm^2 s) in 2011–2013 [3]. Meanwhile, the photon return ranges from 55 to 140 ph/(cm^2 s) with an equivalent V magnitude of 9.5 to 10.5 mag at the zenith on a Keck telescope [4]. Even latest generation of guide star lasers used, the photon return in subaperture per frame is possibly low, and the LGS AOS would operate at a low SNR, which mainly limits the performance of the LGS AOS. To increase the SNR, an electron multiplying (EM) charge-coupled device (EMCCD) is used to suppress the read-out noise with an EM gain and to reduce the effects of dark-current noise by cooling. Thus, the photon noise becomes the main noise. If a method is available that can eliminate the photon noise, LGS detection will become more precise. An LGS spot appears similar to a stick-shaped image, instead of a point image [4,5]. The photon noise error in the LGS spot is bigger than the Airy spot because of the elongation.

In addition, error in detection will be generated because of the mismatch between the imaging and detection wavebands. The subaperture diameter of the SHWFS is designed according to the imaging waveband, which is usually in the J, H, or K band. However, the detection wavelength of a sodium LGS is always 589 nm. The diameter of the subaperture is three or four times larger than r_0 at a wavelength of 589 nm. Therefore, not only tip–tilt but also high-order aberrations are present in one sub aperture such as shown in Fig. 1. Then, the detection accuracy will decrease because of the effect of high-order aberrations.

Many centroid algorithms have been considered for wavefront detection of the LGS, such as the center of gravity (COG), quad cell (QC), matched filter (MF) [5–7], correlation method (CM) [8,9], and weighted COG (WCOG) [10–12]. The QC method works only for weak turbulence and is efficient for a noise detector under low-flux conditions [13]. The MF method works only when the spot image is a shifted copy of a reference image and the amount of shift is small [5–7]. Among these algorithms, the WCOG and CM yield fair performance and have a large dynamic range. The WCOG reduces the effects of noise using the weighting function, a time-averaged image. For the CM, the average image is used as a reference image. Because the photon noise follows a Poisson distribution, these methods based on filters cannot perfectly

* Corresponding author.
E-mail address: caozlok@ciomp.ac.cn (Z. Cao).

https://doi.org/10.1016/j.optcom.2018.05.015
Received 6 January 2018; Received in revised form 8 March 2018; Accepted 6 May 2018
Available online 18 May 2018

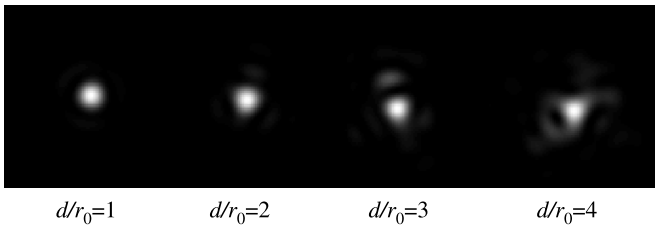

Fig. 1. The point spread function of different strength of turbulence.

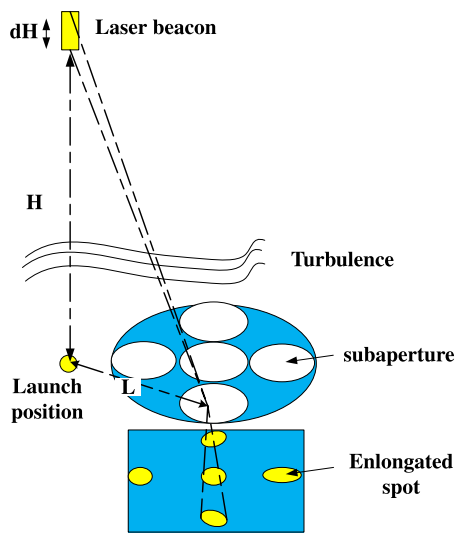

Fig. 2. Schematic diagram of the LGS system.

eliminate the effect of the photon noise. In the present study, the Poisson distribution of the photon noise is considered to reduce the photon-noise effect. We have known well that no centroid algorithm can remove the effect of high-order aberrations. In this paper, we propose a new method to simultaneously reduce the effects of the high-order aberrations in the subaperture and the photon noise.

2. Modeling the elongation spot

To investigate the wavefront detection of the LGS, an LGS model is developed, as shown in Fig. 2.

The LGS elongation is calculated by [11]

$$\theta_{elo} = \frac{LdH}{H(H+dH)} \tag{1}$$

where L is the distance between the subaperture and the launched position, H is the height of the LGS, and dH is the thickness of the sample. Single and bi-model profiles are considered for a sodium laser beacon. The single model is centered at an altitude of 90 km with full width half maximum (FWHM) of 10 km. The two peaks of the bi-modal profile are centered at 84 and 94.5 km with FWHM values of 8.24 and 2.35 km, respectively.

$$\rho(H) = \begin{cases} \exp\left[-\frac{(H-90)^2}{10^2}\right]; & \text{Single model profile} \\ \exp\left[-\frac{(H-84)^2}{8.24^2}\right] + \exp\left[-\frac{(H-94.5)^2}{2.35^2}\right]; & \text{Bi-model profile.} \end{cases} \tag{2}$$

The non-elongated axis of the beam is 1.1″ with condition of *seeing* = 1″ and the subaperture diameter is 0.5 m; these conditions are the same as those in the European extremely large telescope [10,14]. The high resolution image is a convolution process of LGS and PSF in subaperture [9]. And then, images without noise and turbulence of the LGS spot at the resolution of a subaperture can be simulated, as shown in Fig. 3.

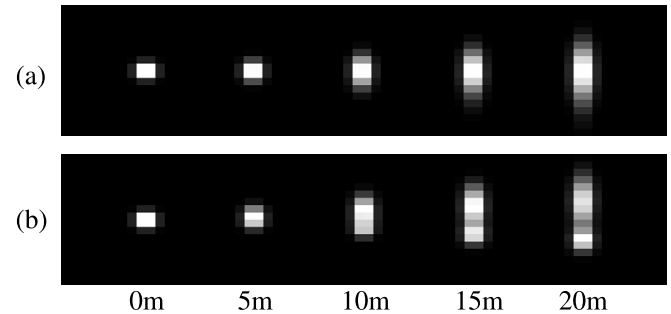

Fig. 3. Spots with different L values. (a) First line: single sodium profile. (b) Second line: bi-model sodium profile.

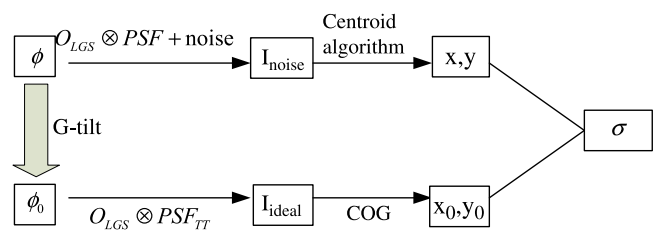

Fig. 4. Flow diagram of the emulation.

The flow diagram of the simulation is shown in Fig. 4.

O_{LGS} denotes the object of the LGS, and PSF_{TT} represents the point spread function (PSF) of the average tip–tilt part in wavefront ϕ. First, turbulence phase ϕ is generated, and an image is obtained by the LGS with a sodium profile convoluted with the PSF of the turbulence phase. Then, the noise image is obtained from the convoluted image pulse noises and degraded to an image with low resolution in the subaperture. The centroid (x, y) of the image is calculated using different centroid algorithms. At the same time, the G-tilt, which is the average phase gradient over the subaperture corresponding to the true spot centroid, is calculated to generate average tip–tilt phase ϕ_0. The ideal image without noise and influenced only by the tip–tilt is obtained from the convolution process and is degraded to a low-resolution image. The true spot centroid (x_0, y_0) is calculated using COG to an ideal image. Finally, centroid error σ is calculated by the following:

$$\sigma = \sqrt{\left\langle (x-x_0)^2 + (y-y_0)^2 \right\rangle}. \tag{3}$$

3. Theory of the method

First, the effects of high-order aberrations are analyzed for wavefront detection of the LGS. In a subaperture, tip–tilt may be detected using the displacement of the LGS spot. However, the high-order aberrations will degrade the spot image, and the detection accuracy will then be reduced. To conveniently analyze the effects of the high-order aberrations, the distorted PSF of one subaperture is treated as a combination of PSF_{TT} and PSF of high-order aberrations PSF_{HA}. Thus, the spot image in subaperture can be expressed as

$$\begin{aligned} I &= O_{LGS} \otimes PSF \\ &= O_{LGS} \otimes PSF_{TT} \otimes PSF_{HA} \\ &= I_{ideal} \otimes PSF_{HA} \end{aligned} \tag{4}$$

where O_{LGS} is the object of the LGS and I_{ideal} is the image of the LGS without high-order aberrations. We can see that if I_{ideal} can be obtained, the slope of the wavefront can be accurately computed. Furthermore, I

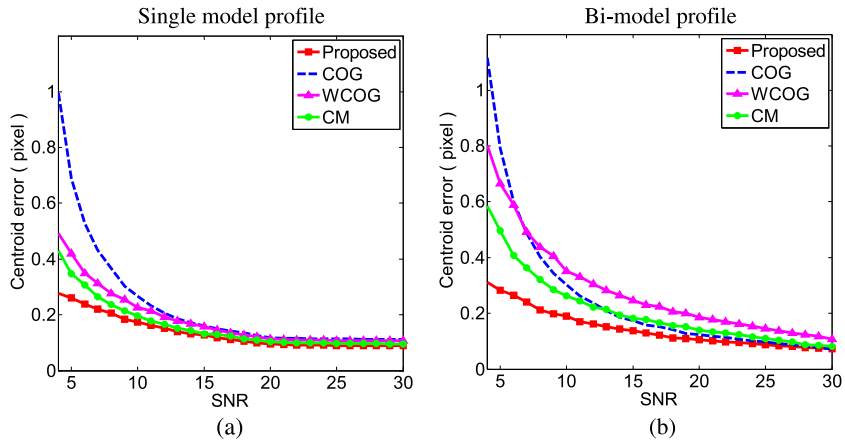

Fig. 5. Performance of different method for different SNR. $L = 10$ m.

will be degraded by the photon noise, and degraded image I_{noise} obeys the Poisson probability

$$P(I_{noise}) = \prod_{1}^{N} \frac{(I_i)^{I_{i\text{-}noise}}}{I_{i\text{-}noise}!} \exp(-I_i) \tag{5}$$

where N is the total number of pixels in one subaperture and the subscript, i, represents the ith pixel. I_i is the intensity of the ith pixel. The $I_{i\text{-}noise}$ is the intensity of the ith pixel in noisy image, I_{noise}. Substituting Eq. (4) into it, Eq. (5) may be rewritten as

$$P(I_{i\text{-}noise} \,|\, I_{i\text{-}ideal}) = \prod_{1}^{N} \frac{(PSF_{HA} \otimes I_{i\text{-}ideal})^{I_{i\text{-}noise}}}{I_{i\text{-}noise}!} \times \exp(-PSF_{HA} \otimes I_{i\text{-}ideal}). \tag{6}$$

The $I_{i\text{-}ideal}$ is the intensity of the ith pixel in ideal image, $I_{i\text{-}ideal}$. Because I_{noise} contains all information of I_{ideal}, the maximum likelihood estimation of I_{ideal} can be obtained from I_{noise}. The maximum likelihood function can be expressed as

$$\begin{aligned} L\left(\tilde{I}_{ideal}\right) &= -\ln\left(P(I_{noise} \,|\, I_{ideal})\right) \\ &= \sum \left\{ -I_{i\text{-}noise} * \ln\left(PSF_{HA} \otimes I_{i\text{-}ideal}\right) \right. \\ &\quad \left. + PSF_{HA} \otimes I_{i\text{-}ideal} + \ln(I_{i\text{-}noise}!) \right\}. \end{aligned} \tag{7}$$

The estimated image and PSF_{HA} could be got by solving the extreme value of maximum likelihood function.

$$\begin{cases} \dfrac{\partial L}{\partial I_{ideal}} = 0 \\ \dfrac{\partial L}{\partial PSF_{HA}} = 0. \end{cases} \tag{8}$$

Eq. (8) can be solved by using the Richardson–Lucy algorithm [15].

$$PSF_{HA}{}^{m+1}(x,y) = \left\{ \left[\frac{I_{noise}(x,y)}{PSF_{HA}{}^{m}(x,y) \otimes I_{ideal}{}^{m}(x,y)} \right] \otimes I_{ideal}{}^{m}(-x,-y) \right\} \times PSF_{HA}{}^{m}(x,y) \tag{9}$$

$$I_{ideal}{}^{m+1}(x,y) = \left\{ \left[\frac{I_{noise}(x,y)}{PSF_{HA}{}^{m}(x,y) \otimes I_{ideal}{}^{m}(x,y)} \right] \otimes PSF_{HA}{}^{m}(-x,-y) \right\} \times I_{ideal}{}^{m}(x,y) \tag{10}$$

where m is the number of iteration times. The initial estimated PSF_{HA} is a 3 by 3 matrix of ones. Because I_{ideal} does not suffer from the effects of the photon noise and high-order aberrations, the centroid of the LGS spot can be accurately calculated using the COG. Therefore, we can find that the effects of photon noise and high-order aberrations of the atmospheric turbulence can be simultaneously eliminated using the proposed method. To guarantee a high computation speed, only once iteration is performed in this study. Although an ideal image could not certainly be obtained by once iteration, the estimated image is closer to the ideal image than the original image. We use the Monte Carlo method to study this image because the centroid error of the proposed method is difficult to express by equations.

4. Monte Carlo simulation

The effects of the photon noise are first simulated. The field of view (FOV) of the subaperture is designed to be 18″, and 18 × 18 pixels are included in one subaperture. For the CM, the peak of the correlation function is determined using a threshold of 0.3. The time-average image is the reference image in CM and weighted function in WCOG. The SNR could be expressed as

$$\text{SNR} = \frac{N_p}{\sqrt{N_p + N_D\left[{n_B}^2 + (\frac{e_n}{G})^2\right]}}, \tag{11}$$

where N_p is the number of detected photons per subaperture, N_D is the number of pixels in a subaperture, n_B is the number of dark current and detected background photoelectrons per subaperture, e_n is the read-out noise in the electrons per pixel, and G is the gain. In this paper, we use EMCCD to detect the LGS spot, and n_B could be ignored by cooling. The influence of the read-out noise is very small compared with the EM gain. When the latest generation of guide star laser is used, the photodetection events per subaperture per frame is normally supposed to 900, and pessimistically supposed to 250, so the SNR is range from to 15 to 30 [14].

To study the influence of the photon noise, the wavefront at the pupil is assumed to be a plane, and I_{noise} is only influenced by the photon noise. The performance of different method with different SNR is shown in Fig. 5. The results show that the centroid error is a big difference between different sodium profiles. There is more photon noise in LGS spot of bi-model profile due to more complex intensity distribution. At single model profile, the distribution of intensity is relatively regular, and the methods based on filter, WCOG and CM, perform better than COG. However, at bi-model profile, these filter methods perform worse, because the filters are not suitable for spot with more complex intensity distribution.

We demonstrate that at different SNRs, the centroid error of the proposed method is less than those of the other methods, and the proposed method is better at smaller SNRs. The slope calculation of the proposed method is COG, and before the calculation the photon noise reduction processing is done on LGS spot. The filter methods change the spot shape, so these filter method could not be suitable for more complex LGS spot image.

To study performance in difference subaperture, the performance of different method with different L is shown is Fig. 6. The photon

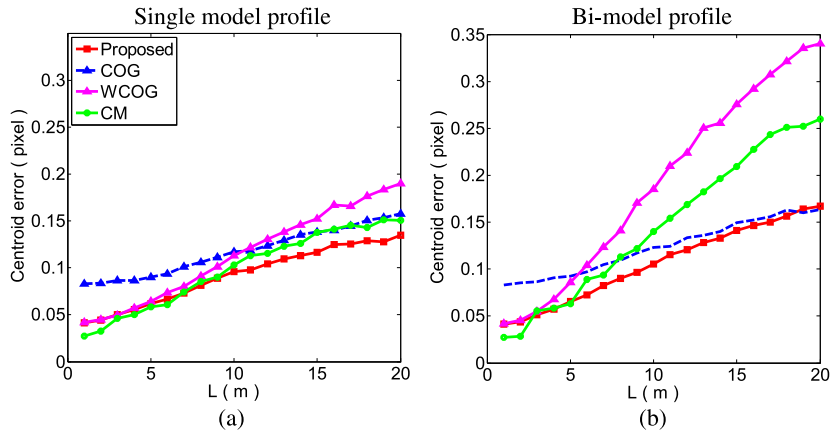

Fig. 6. Performance of different method for different L . $SNR = 20$.

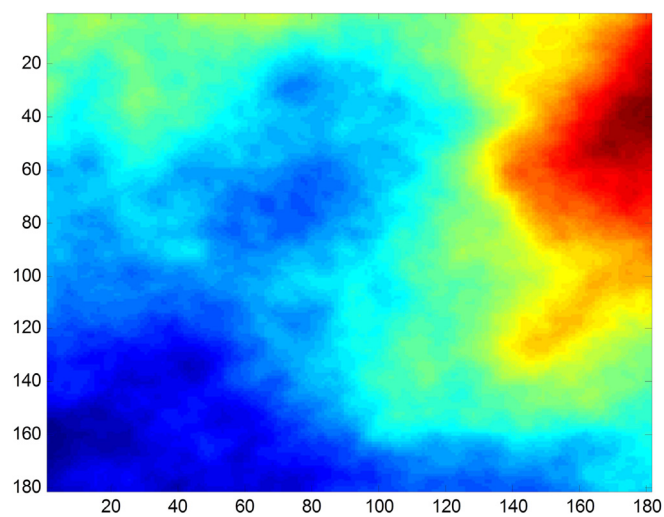

Fig. 7. Kolmogorov phase screens in one subaperture.

noise would grow with the elongation and complicit of distribution of spot. The performance of WCOG is mainly determined by the FWHM of weighted function. When the elongation grows, the FWHM of average image is not always the optimal. When the L is small, the spot is relatively simple and the filter methods perform well. The Figs. 5 and 6 show that our method could better reduce the photon noise than the other methods especially at lower SNR and larger elongation, but could not eliminate photon noise entirely. Our method is based on the Poisson distribution, which can better reduce the photon noise, instead of the filter method.

Elimination of the high-order aberrations due to atmospheric turbulence is also performed using the proposed method. To study the influence of turbulence only, the image is considered to contain no noise, whether photon or read-out noise. The turbulence phase is randomly generated with 181 ×181 grid points in one sub aperture such as Fig. 7. The method of generating turbulence phase is the Fourier transform method augmented with subharmonics [16].

I_{noise} is only influenced by the turbulence. The centroid errors of the above-mentioned methods are shown in Fig. 8, which reveals that the performance of the proposed method is better than that of the other methods at different r_0 values. At $r_0 = 13$ cm, the centroid error of the proposed method is less than those of the other methods. The error of our method slowly decreases with r_0 and slightly increases with the increment in distance L , which means that our method is robust to high-order aberration in the subaperture and under elongation. The errors of the WCOG and CM dramatically decrease, which means that the high-order aberrations in the subaperture badly influence the precision. When r_0 is small, the weighted function of the WCOG obscures the detail of the spot image, and the reference image in the CM decreases the frequency, which is supposed to exist. Finally the WCOG and CM are not suitable for turbulence during storms.

Theoretically, our method separates the spot image into an image influenced only by the average tip–tilt and the distorted PSF, which is caused by high-order aberration. In fact the capacity of eliminating high-order aberration is limited. The less degraded image is used in estimating the slope, the better method performs.

By assuming that both photon noise and high-order aberrations exist, the centroid calculation accuracy of the proposed and other methods is evaluated. As shown in Fig. 9, $SNR = 20$ and $r_0 = 13$ cm are selected for the simulation.

Fig. 9 shows that when L is less than 10 m, the centroid error of the WCOG and CM is smaller than COG. It means that when the diameter of the aperture of telescope is smaller than 10 m with lateral laser projection or smaller than 20 m with central laser projection, filter method performs better than COG. And the WCOG and CM would not be suitable for large aperture telescope whose max elongation distance is larger than 10 m. The centroid error of the proposed method is smaller than those of the other methods in both the single and bi-model profile. And variation tendency with L of the proposed method is similar to that of COG. And the proposed method keeps the characters of COG. The reason why is that our method is not based on filter and do not change the LGS spot shape.

In order to known how close the estimated image to the ideal image after once iteration, under the single model profile, the results of once iteration are shown in Figs. 10 and 11. The results show that the intensity distribution of image after once iteration is obviously closer to that of ideal image. The estimated image is with less photon noise and high-order aberrations.

We simulate a simple open-loop reconstruction for practical astronomical application. The parameters are listed in Table 1.

The LGS could not detect information of tip–tilt. And focus could not be detected precisely due to cone effect, which is always detected by truth sensor. We generate 1000 random Kolmogorov phase screens that remove the global tip–tilt and focus. The above-mentioned methods are used for the detection and reconstruction using 100 Zernike models. The root mean square (RMS) of the residual wavefront is calculated and expressed in nanometer units. And the fitting error is removed. The array of the LGS spot in the single-model profile and one of the Kolmogorov phase screens are shown in Fig. 12, and the errors are shown in Fig. 13. For the single model, the residual RMS using our method is approximately 67 nm, which is 12%, 46%, and 31% lower than that of the COG, WCOG, and CM, respectively. For the bi-model profile, the residual RMS using our method is approximately 70 nm,

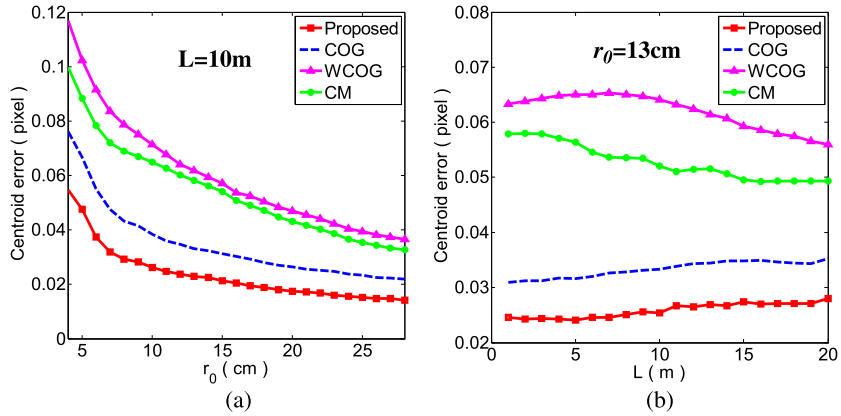

Fig. 8. Performance comparison of the different methods for various r_0 and L values.

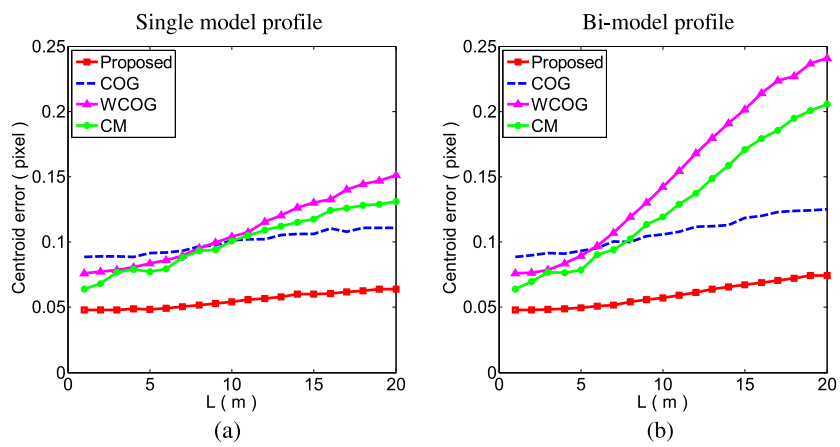

Fig. 9. Performance comparison of the different methods for various L values under the condition of $r_0 = 13$ cm and $SNR = 20$.

Table 1
Parameters used for reconstruction simulation.

Parameters	Values
Diameter of telescope	20 m
No. of subapertures across D	40 × 40
Subaperture FOV	18 × 18 pixels
Pixel scale	1 arcsec/pixel
Launch position	Lateral laser projection
Turbulence	$r_0 = 13$ cm
SNR	20
Detection camera	Andor iXon 888
	RON < 1e⁻ with EM gain

Table 2
Computing time for different method. Computer: Inter(R) Core(TM) i5-4570, CPU @3.2 GHz, Physical Memory 1886 MB, Virtual Memory 754 MB, Executive Software: Matlab.

Method	COG	WCOG	CM	Proposed
Computation time (μs)	125	140	1313	1364

which is 10%, 52%, and 38% lower than that of the COG, WCOG, and CM, respectively.

We also did some test about computing time, and the result is shown in Table 2.

The computation time remains a problem to be studied. Our preliminary scheme is to develop a faster iteration or a simpler calculation process. For now, the computation time is basically in accordance with the correlation method.

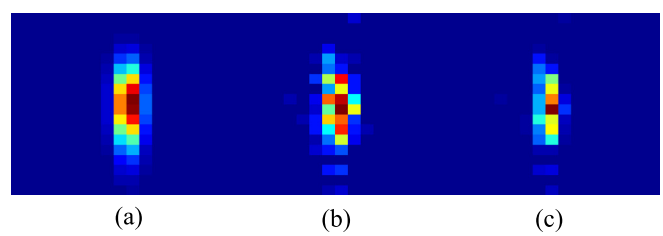

Fig. 10. The result of once iteration about photon noise. $L = 20$ m, $SNR = 20$. (a) the ideal image at random position; (b) the image with photon noise; (c) the image after once iteration.

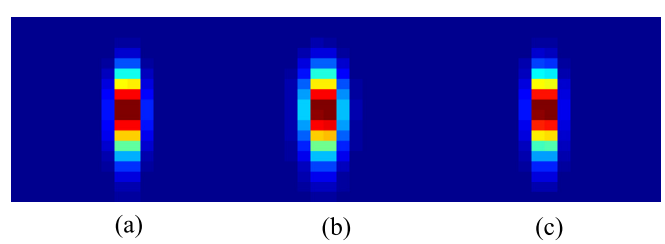

Fig. 11. The result of once iteration about turbulence. $L = 20$ m, $r_0 = 13$ cm. (a) the ideal image at random position; (b) the image with turbulence; (c) the image after once iteration.

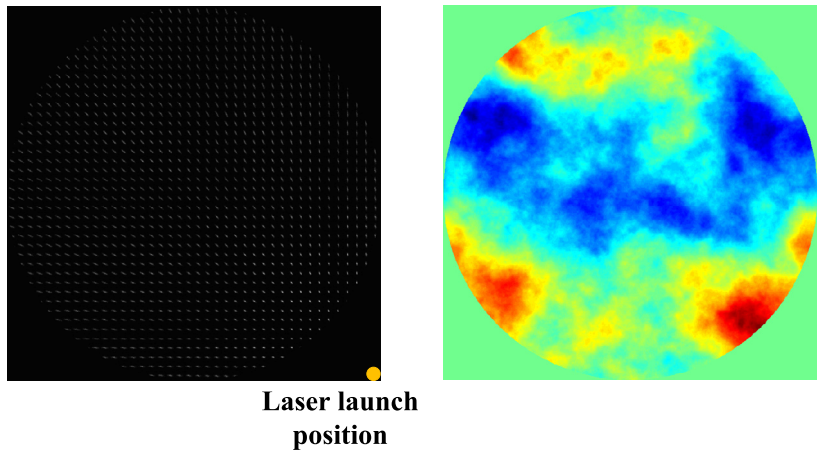

Fig. 12. Array of the LGS spot and one of the Kolmogorov phase screens.

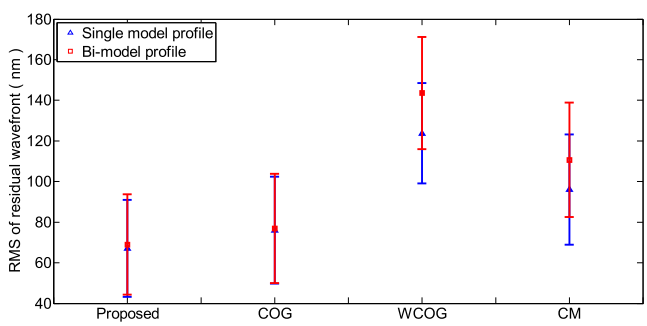

Fig. 13. Error bars of the RMS of the residual wavefront using the different methods.

5. Conclusions

We have proposed a method to well estimate the slope of an LGS spot. This method could effectively reduce the photon noise and eliminate high-order aberrations in a subaperture when an EMCCD is used, especially at low SNR and in a large telescope. The reconstruction simulation indicates that our method could obtain the smallest RMS of the residual wavefront.

The centroid algorithm based on a filter could simply deal with the LGS spot and reduce the errors to a certain degree. The performance of the filter methods relies on the filter function, weighted function in the WCOG, or the reference image in the CM. These filter functions would obscure the details of the spot, resulting in error. Therefore, obtaining a suitable filter function is very important. On the other hand, our method is based on the Poisson distribution to reduce the photon noise and high-order aberration in the subapertures, which does not damage the LGS spot details.

Using a different peak-determination method in the CM could possibly improve the performance. Further effort is needed so that our proposed method could be applied to LGS AO, such as improvement in the computation time. Our method is also valuable in obtaining high-resolution images in other adaptive optics applications.

Acknowledgment

We thank the State Key Laboratory of Applied Optics for the support.

Funding

National Natural Science Foundation of China with Grant Numbers 11174274, 11174279, 61205021, 11204299, 61475152, and 61405194.

References

[1] Peter Wizinowich, Progress in laser guide star adaptive optics and lessons learned, Proc. SPIE 8447 (2012) 84470D-84470D-14.

[2] Martin J. Booth, Adaptive optical microscopy: the ongoing quest for a perfect image, Light: Sci. Appl. 3 (2014) e165.

[3] Benoit Neichel, François Rigaut, Fabrice Vidal, Marcos A. van Dam, Vincent Garrel, 1. Eleazar Rodrigo Carrasco, Peter Pessev, Claudia Winge, Maxime Boccas, Céline d'Orgeville, Gustavo Arriagada, Andrew Serio, Vincent Fesquet, William N. Rambold, Javier Lührs, Cristian Moreno, Gaston Gausachs, Ramon L. Galvez, Vanessa Montes, Tomislav B. Vucina, Eduardo Marin, Cristian Urrutia, Ariel Lopez, Sarah J. Diggs, Claudio Marchant, Angelic W. Ebbers, Chadwick Trujillo, Matthieu Bec, Gelys Trancho, Peter McGregor, Peter J. Young, Felipe Colazo, Michelle L. Edwards, Gemini multi-conjugate adaptive optics system review II: Commissioning, operation and overall performance, Mon. Not. R. Astron. Soc. 000 (2014) 1–20.

[4] Peter L. Wizinowich, David Le Mignant, Antonin H. Bouchez, Randy D. Campbell, Jason C.Y. Chin, Adam R. Contos, Marcos A. van Dam, Scott K. Hartman, Erik M. Johansson, Robert E. Lafon, Hilton Lewis, Paul J. Stomski, Douglas M. Summers, The W. M. Keck Observatory Laser Guide Star Adaptive Optics System: Overview, Publications of the Astronomical Society of the Pacific, 2006, pp. 297–309.

[5] Olivier Lardi`ere, Rodolphe Conan, Colin Bradley, Colin Bradley, Glen Herriot, Kate Jackson, Laser–Guide–Star wavefront sensing for TMT: Experimental results of the Matched Filtering, Proc. SPIE 7015 (2008).

[6] Luc Gillesa, Brent Ellerbroek, Laser guide star Shack -Hartmann wavefront sensor modeling: matched filtering, wavefront sensor nonlinearity, and impact of sodium layer variability for the Thirty Meter Telescope, Proc. SPIE 6272 (2006).

[7] Luc Gilles, Brent Ellerbroek, Shack–Hartmann wavefront sensing with elongated sodium laser beacons: centroiding versus matched filtering, Appl. Opt. 45 (25) (2006).

[8] Olivier Lardi`ere, Rodolphe Conan, Richard Clare, Colin Bradley, Norbert Hubin, Performance comparison of centroiding algorithms for laser guide star wavefront sensing with extremely large telescopes, Appl. Opt. 49 (31) (2010).

[9] Damien Gratadour, Eric Gendron, Thierry Fusco, Gerard Rousset, Serge Meimon, Comparing centroiding methods for Shack–Hartmann wavefront sensing with laser guide stars on an ELT, Proc. SPIE 7736 (2010).

[10] L. Schreiber, I. Foppiani, C. Robert, E. Diolaiti, J.-M. Conan, M. Lombini, Laser guide stars for extremely large telescopes: efficient Shack–Hartmann wavefront sensor design using the weighted centre-of-gravity algorithm, Mon. Not. R. Astron. Soc. 396 (2009) 1513–1521.

[11] M. Nicolle, T. Fusco, G. Rousset, V. Michau, Improvement of Shack–Hartmann wavefront sensor measurement for extreme adaptive optics, Opt. Lett. 29 (2004).

[12] Damien Gratadour, Eric Gendron Gerard Rousset, Symmetrically weighted center of gravity for Shack - Hartmann wavefront sensing on a laser guide star, Proc. SPIE 7736 (2010).

[13] M. Lombini, I. Foppiani, L. Schreiber, E. Diolaiti, G. Bregoli, G. Cosentino, Design of the multiple Laser Guide Stars wavefront sensor prototype for the EELT, Proc. SPIE 8447 (2012).

[14] C. Boyer, B. Ellerbroek, L. Gilles, et al., The TMT laser guide star facility, Adapt. Opt. Extremely Large Telesc. (2010).

[15] D. Biggs, M. Andrews, Interative blind deconvolution of extended objects, in: International Conference on Image Processing, Proceedings, Vol. 2, IEEE, 1997, pp. 454–457.

[16] R.G. Lane, A. Glindemann, J.C. Dainty, Simulation of a Kolmogorov phase screen, Waves Random Media 2 (1992) 209–224.